Accurate Time-dependent Wave Packet Calculations for the O(+)+H2 → OH(+)+H Ion-Molecule Reaction.

ARTICLE *in* THE JOURNAL OF PHYSICAL CHEMISTRY A · MARCH 2015

Impact Factor: 2.69 · DOI: 10.1021/acs.jpca.5b00815 · Source: PubMed

7 AUTHORS, INCLUDING:

Niyazi Bulut
Firat University
40 PUBLICATIONS **282** CITATIONS
SEE PROFILE

Jesus F Castillo
Complutense University of Madrid
76 PUBLICATIONS **2,064** CITATIONS
SEE PROFILE

Octavio Roncero
Spanish National Research Council
142 PUBLICATIONS **2,826** CITATIONS
SEE PROFILE

THE JOURNAL OF PHYSICAL CHEMISTRY A

Article

pubs.acs.org/JPCA

Accurate Time-Dependent Wave Packet Calculations for the $O^+ + H_2 \rightarrow OH^+ + H$ Ion–Molecule Reaction

N. Bulut,[†] J.F. Castillo,[‡] P. G. Jambrina,[‡] J. Kłos,[§] O. Roncero,[∥] F. J. Aoiz,[‡] and L. Bañares*[,‡]

[†]Department of Physics, Firat University, 23169 Elazığ, Turkey

[‡]Departamento de Química Física I, Facultad de Ciencias Químicas, Universidad Complutense de Madrid (Unidad Asociada I+D+i CSIC), 28040 Madrid, Spain

[§]Department of Chemistry and Biochemistry, University of Maryland, College Park, Maryland 20742-2021, United States

[∥]Departamento de Física Atómica, Molecular y de Agregados, Instituto de Física Fundamental, CSIC, C/Serrano, 123, 28006 Madrid, Spain

Supporting Information

ABSTRACT: Accurate quantum reactive scattering time-dependent wave packet close-coupling calculations have been carried out to determine total reaction probabilities and integral cross sections for the $O^+ + H_2 \rightarrow OH^+ + H$ reaction in a range of collision energies from 10^{-3} eV up to 1.0 eV for the H_2 rovibrational states ($v = 0$; $j = 0, 1, 2$) and ($v = 1$; $j = 0$) using the potential energy surface (PES) by Martínez et al. As expected for a barrierless reaction, the reaction cross section decays rapidly with collision energy, E_c, following a behavior that nearly corresponds to that predicted by the Langevin model. Rotational excitation of H_2 into $j = 1, 2$ has a very moderate effect on reactivity, similarly to what happens with vibrational excitation below $E_c \approx 0.3$ eV. However, at higher collision energies the cross section increases notably when H_2 is promoted to $v = 1$. This effect is explained by resorting to the effective potentials in the entrance channel. The integral cross sections have been used to calculate rate constants in the temperature range 200–1000 K. A good overall agreement has been found with the available experimental data on integral cross sections and rate constants. In addition, time-independent quantum mechanical and quasi-classical trajectory (QCT) calculations have been performed on the same PES aimed to compare the various methodologies and to discern the detailed mechanism of the title reaction. In particular, the analysis of individual trajectories has made it possible to explain, in terms of the coupling between reagent relative velocity and the topography of the PES, the presence of a series of alternating maxima and minima in the collision energy dependence of the QCT reaction probabilities for the reactions with $H_2(v=0,1,j=0)$, which are absent in the quantum mechanical calculations.

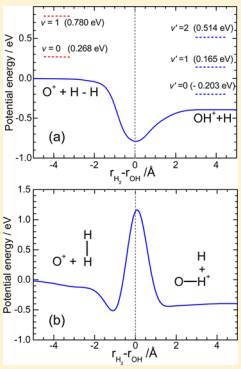

1. INTRODUCTION

Ion–molecule elementary reactions have fundamental interest in the physics and chemistry of interstellar clouds, planetary ionospheres, plasmas, and combustion processes.[1,2] The exothermic reaction

$$O^+(^4S) + H_2(^1\Sigma_g^+) \rightarrow OH^+(^3\Sigma^-) + H(^2S) \qquad \Delta H_0^\circ = -0.54 \text{ eV} \tag{1}$$

is known to be important for the evolution of dense interstellar clouds, where the OH^+ products react with H_2 molecules to form H_2O^+ and H_3O^+ molecular ions. This reaction, which is a prototype of a moderately exothermic ion–molecule reactive system involving H atom transfer, has been studied both experimentally[3−9] and theoretically.[10−16]

A variety of experimental techniques, such as ion beam-static cell with angular resolution,[17,18] flowing afterglow,[3] ion-cyclotron resonance,[4] selected ion flow tube,[5,6] and guide ion beam,[7−9] have been applied to the study of the title reaction and isotopic variants, aimed to determine rate coefficients, cross sections, and product angle-recoil velocity distributions. The measured thermal rate coefficient at 300 K ranged from 1.2×10^{-9} to 2×10^{-9} cm^3 s^{-1}, which agrees fairly well with the simple prediction based on the Langevin model.[19,20] Burley et al.[7] carried out extensive and precise measurements of the reaction cross section as a function of the collision energy in the 0.01–10 eV interval. They found that below 0.3 eV, the excitation function, i.e., the collision energy dependence of the integral cross section $\sigma_r(E_c)$, could be described by the equation $\sigma_r(E_c) = 16$ Å^2 eV$^{1/2}$ $E_c^{-1/2}$, in almost a perfect agreement with the Langevin model prediction. Using these data, these authors determine a rate coefficient at 300 K $k(T) = 1.67 \times 10^{-9}$ cm^3 s^{-1} as compared with the value of 1.56×10^{-9} cm^3 s^{-1} given by the simple Langevin model.[19,20] Incorporating the anisotropic ion–quadrupole interaction, which is relevant for initial $j \neq 0$, they found a value of 1.61×10^{-9} cm^3 s^{-1}, in slightly better agreement with the measured value. At collision energies above 0.3 eV, the

Special Issue: Dynamics of Molecular Collisions XXV: Fifty Years of Chemical Reaction Dynamics

Received: January 26, 2015
Revised: March 21, 2015

DOI: 10.1021/acs.jpca.5b00815
J. Phys. Chem. A XXXX, XXX, XXX–XXX

experimental cross section clearly deviated from the Langevin prediction with a larger negative slope in the $\sigma_r(E_c)$ and smaller pre-exponential factor. Using phase space model arguments, the authors attributed the deviation from the Langevin model at $E_c \geq 0.3$ eV to an increase of nonreactive collisions due to angular momentum constraints in the exit channel.[7]

From a theoretical point of view, an analytical global potential energy surface (PES) for the OH_2^+ system in the ground electronic state $1^4A'$ was developed by Martínez et al.[10] by fitting around 600 points calculated at coupled cluster with single and double excitations and perturbative treatment of triple excitations, CCSD(T), *ab initio* theory using a Dunning cc-pVQZ basis set. The *ab initio* points were calculated in selected representative regions of the PES with $C_{\infty v}$, C_s and C_{2v} symmetries. These calculations showed that reaction 1 may take place along a collinear minimum energy path O^+−HH of the lowest quadruplet $1^4A'$ PES without surmounting any energy barrier above reactants. Along this pathway there is a minimum of $^4\Sigma^-$ symmetry in the OH^+ + H product valley that corresponds to the absolute minimum of the system. When the reactants approach C_{2v} geometry, a crossing between the ground and first excited state PESs takes place. When the symmetry of the system decreases (C_s symmetry near to C_{2v} symmetry), this crossing leads to an avoided crossing, as both PESs become A″ symmetry. This avoided crossing generates an energy barrier of approximately 2.9 eV on the ground state PES near the C_{2v} symmetry, which corresponds to the barrier for the insertion process of O^+ into the H−H bond. At low and moderate collision energies the reaction is thus expected to occur adiabatically on the ground state PES,[10] whereas at high collision energies (≥2.9 eV), the first excited state PES and the ground state PES for configurations far from linearity (near a C_{2v} symmetry) are also expected to contribute to the reactivity.

There have been several dynamics calculations carried out for the title reaction[10−16] on the OH_2^+ PES of Martínez et al. (MMG PES).[10] Quasiclassical trajectory (QCT) calculations were performed by Martínez et al.[10,11] for the title reaction and the HD and D_2 isotopic variants. Integral cross sections in the collision energy range 0.01−0.6 eV, considering the reactants in thermal equilibrium at 300 K, and rate constants in the temperature interval 200−1400 K were calculated. The excitation functions were found to be in good general agreement with the available experimental values by Burley et al.[7] The loss of reaction efficiency at collision energies above 0.3 eV was attributed by these authors to a decrease in the number of reactive trajectories evolving through the collinear O^+−HH path.[11] The corresponding QCT rate constant at 300 K was found to be 1.71×10^{-9}, in very good agreement with the already mentioned experimental value.[7]

In a later work, accurate time-independent quantum mechanical (TIQM) close-coupling calculations using hyperspherical coordinates were carried out for the $O^+ + H_2(v=0,j=0)$ reaction and compared with QCT calculations on the same PES in the 0.04−1.24 eV collision energy range.[12] The agreement between the TIQM and QCT integral cross sections was found to be good at collision energies below 0.2 eV. At collision energies between 0.2 and 0.6 eV, the QCT cross sections were somewhat lower than the TIQM cross sections but the differences were reduced for energies above 0.6 eV. The discrepancies at low collision energies were tentatively attributed to the inability of the trajectories to describe the reactivity of the system through OH_2^+ geometries not far from the C_{2v} symmetry, where tunneling effects should be noticeable. Interestingly, the QCT cross sections for the $O^+ + H_2(v=0,j=1)$ reaction and the previous QCT results considering a thermal (T = 300 K) internal state distribution of H_2[10] were very close to the TIQM cross sections for the $O^+ + H_2(v=0,j=0)$ reaction, which indicates a mild dependence of reactivity on reagent rotational excitation.

Subsequently, time-dependent quantum mechanical real wave packet (TDQM-RWP) calculations within the centrifugal sudden (CS) approximation, which neglected the Coriolis coupling, were performed by the same group[13] for total angular momentum $J > 0$ for the $O^+ + H_2(v=0,j=0)$ reaction and its isotopic variants. A relatively good agreement was found between the excitation functions calculated using the TDQM-RWP-CS and TIQM methodologies. However, both methods yielded somewhat different reaction probabilities, although the differences seemed to cancel in the partial wave summation in the integral cross section calculation.

A comprehensive time-dependent quantum mechanical wave packet study of the $O^+ + H_2(v=0,j=0)$ reaction and its isotopic variants, considering Coriolis coupling (TDWP-CC) and using the CS approximation (TDWP-CS), has been performed recently by Xu et al.[15] on the MMG PES.[10] These calculations were carried out using the same TDWP methodology and thus they provide a fair means for comparison between the CC and CS approaches. It should be recalled that the previous CS calculations were done using time-dependent theory (TD-RWP-CS),[13] whereas the Coriolis coupling calculations were performed using a time-independent method (TIQM).[12] The calculated TDWP-CC and TDWP-CS reaction probabilities and integral cross sections for the $O^+ + H_2(v=0,j=0)$ reaction by Xu et al.[15] were essentially coincident with the TIQM[12] and TD-RWP-CS[13] results, respectively, as should be expected. It was found that the CS approximation overestimates or slightly underestimates the integral cross sections at high collision energies (E_c > 0.4 eV) or low collision energies (E_c < 0.4 eV), respectively, for the $O^+ + H_2(v=0,j=0)/D_2(v=0,j=0)$ reactions. The main conclusion of that work is that the Coriolis coupling effect plays a significant role in the $O^+ + H_2$ reaction and its isotopic variants.

Very recently, accurate TDWP-CC calculations were carried out by some of us for the $O^+ + H_2(v=0,j=0,1)$ reaction[16] on the MMG PES.[10] Total integral cross sections and state-to-state rate constants were obtained and compared with the existing experimental data. The main aim of those reactive calculations, along with radiative pumping and inelastic collisions, was to improve the reliability of chemical and radiative transfer models for OH^+ applied to astrophysical environments.[16]

In the present work, we have employed the same accurate TDWP-CC as in previous works[16,21−23] as implemented in the MADWAVE3 code. We have used it to calculate total reaction probabilities, integral cross sections and rate constants for the title reaction with the H_2 molecule in selected initial rovibrational states (v = 0, j = 0, 1, 2 and v = 1, j = 0) in the 0.001−1.0 eV collision energy range on the MMG PES.[10] In addition, TIQM reactive scattering calculations have been conducted on the same PES for comparison with the corresponding wave packet results to check their accuracy at the lowest collision energies. QCT calculations have also been carried out to extract some insights on the dynamical mechanism of the title reaction and elucidate those effects which are genuinely quantum mechanical. The present calculations provide an extension of previous accurate quantum dynamics computations,[12,13,15] which only considered the v = 0, j = 0

DOI: 10.1021/acs.jpca.5b00815
J. Phys. Chem. A XXXX, XXX, XXX−XXX

quantum states of the H_2 molecule and those of the work presented in ref 16. The inclusion of higher H_2 rotational levels, relevant to the thermal distribution at 300 K, allows a more precise comparison with the experimental thermal measurements,[7] as well as a further insight into the reaction dynamics dependence on the initial quantum states of the reagents.

The outline of the paper is as follows: in section 2 we briefly review the time-dependent wave packet close-coupling method and the technical details of the calculations performed in this work. Sections 3 and 4 present the main results and discussions, respectively, and finally, section 5 closes with some concluding remarks.

2. METHODOLOGY

We have employed the TDWP-CC method developed by Roncero and co-workers[21−23] implemented in the MAD-WAVE3 code, which uses either reactant or product Jacobi coordinates to extract the state-to-state **S**-matrix elements. For reactive systems like that considered in this work, it has been demonstrated that given the mass combinations, it is more convenient to use reactant's (r, R, γ) Jacobi coordinates.[21] The initial wave packet that defines the initial state of the reagents at a sufficiently long initial distance, $R = R_0$, at which the interaction potential is negligible, is taken as

$$\Psi^{\alpha}(t=0) = \sum_{\Omega} W^{J\epsilon}_{M\Omega}(\phi,\theta,\chi)\, \chi_{vj}(r)\, \tilde{Y}_{j\Omega}(\gamma) \langle R|g^{J,\epsilon,v,j,\Omega_0}_{\Omega}(t=0)\rangle \tag{2}$$

where $\alpha = J, M, \epsilon, v, j, \Omega_0$, $W^{J\epsilon}_{M\Omega}(\phi,\theta,\chi)$ denotes a parity-adapted basis set that depends on the ϕ,θ,χ Euler angles, $\chi_{vj}(r)$ are the ro-vibrational eigenfunctions of the $H_2(v,j)$ reactant, $\tilde{Y}_{j\Omega}(\gamma)$ are normalized associated Legendre polynomials, ϵ denotes the parity, and $\langle R|g^{J,\epsilon,v,j,\Omega_0}_{\Omega}(t=0)\rangle$ is a real superposition of incoming and outgoing Gaussian functions. The radial variables r and R are described in finite grids of equidistant points, whereas γ is represented by Gauss-Legendre quadrature points. The helicity quantum number Ω, and M are the projections of the total angular momentum, J, on the body-fixed z-axis and the space fixed Z axis, respectively.

The propagation of the wave packet is carried out by means of a modified Chebyshev integrator and a real absorbing function is introduced to avoid reflection at the end of the grid. The relevant parameters used in the method for the title system are given in Table 1.

The parameters used for the wave packet propagation were carefully optimized to get accurate results at energies as low as 1 meV. Initially, this was done for $J = 0$ because the calculations are much less time-consuming and it was later checked for $J > 0$ by mean of calculating the flux on all the possible channels individually, and summing over them. Because the unitarity is not imposed, a good convergence criterion consists in verifying how much the total sum differ from unity. We found a generally good compliance of this requirement for energies >0.1−0.2 eV. The accuracy of the TDWP results was further verified by comparing with those obtained by TIQM calculations at selected angular momentum J, finding an excellent agreement between the two sets of results at energies at low 1 meV. The calculation of reaction probabilities for $J > 0$ would require us to include all possible helicity Ω projections. Because including all Ω projections for high J values is very demanding computationally and not strictly necessary to obtain converged results, the helicity basis has been truncated, so that $|\Omega| \leq \min(J,\Omega_{max})$ with $\Omega_{max} = 7$. This value of Ω_{max} provides convergence of the reaction probabilities for the considered collision energy range in agreement with previous works on the same system.[12,13,15]

Table 1. Parameters Used in the TDWP Calculations (All Distances in Å and Energies in eV)

reactant scattering coordinate R range	$R_{min} = 0.32$; $R_{max} = 36.0$
absorption parameters	$R_{abs} = 16$; $A_R = 10^{-6}$ [a]
no. of grid points in R	620
diatomic coordinate r range	$r_{min} = 0.2$; $r_{max} = 30.0$ [a]
absorption parameters	$r_{abs} = 16$, $A_r = 3 \times 10^{-6}$
no. of grid points in r	256
no. of angular basis functions	160
center of initial wave packet	$R_0 = 13.0$
width of the initial wave packet	$\Delta E = 0.1$
initial translational kinetic energy/eV	$E_c = 0.2$
position of the analysis line	$R'_{\infty} = 11.0$
no. of Chebyshev iterations	50 000
V_{cut}	3.7
E^J_{cut}	5
maximum helicity (reactants), Ω_{max}	7
maximum helicity (products), Ω'_{max}	25

[a]The function used for the absorption has the form $f(X) = \exp\{-A_X[(X - X_{abs})/b]^n\}$ for $X > X_{abs}$ and $f(X) = 1$ elsewhere, with $X \equiv R$ and r, and with $n = 4$ and $b = 2$.

To calculate the **S**-matrix elements corresponding to final states of the OH^+ products, the wave packet is projected on the final state of the products at a separation R'_{∞} between the two moieties to calculate the flux on each channel. To this purpose, the wave packet is transformed from reactants Jacobi coordinates to products, i.e., from (r, R, γ, Ω) to $(r', R'_{\infty}, \gamma', \Omega')$. The specific details on how to obtain the **S**-matrix for high J's including the proper phase to calculate the differential cross section can be found in refs 21, 22, and 24.

To get converged integral cross sections for collision energies up to 1.0 eV, reaction probabilities have been calculated for all partial waves from $J = 0$ up to $J = 30$; from this value, only partial waves multiple of five up to $J = 80$ have been calculated. For the noncalculated intermediate J values, the reaction probabilities have been obtained using a J-shifting based interpolation as described in ref 25. The calculation of the state-to-state integral cross sections (ICS) as a function of collision energy, $\sigma_{v,j\rightarrow v',j'}(E_c)$, requires summing over all the partial wave contributions of the total angular momentum J to the reaction probabilities as[26,27]

$$\sigma_{vj\rightarrow v',j'}(E_c) = \frac{\pi}{k^2}\frac{1}{2j+1}\sum_{J=0}^{J_{max}}(2J+1)[2\min(J,j)+1]P^J_{vj\rightarrow v',j'}(E_c) \tag{3}$$

where $k = (2\mu_R E_c)^{1/2}/\hbar$ is the modulus of the wavenumber vector, and $P^J_{v,j\rightarrow v',j'}(E_c)$ are the state-to-state reaction probabilities at a total angular momentum J, which can be written in terms of the **S**-matrix elements as

$$P^J_{vj\rightarrow v',j'}(E_c) = \frac{1}{2\min(J,j)+1}\sum_{\Omega_0}\sum_{\Omega'}|S^J_{v,j,\Omega_0\rightarrow v',j',\Omega'}|^2 \tag{4}$$

DOI: 10.1021/acs.jpca.5b00815
J. Phys. Chem. A XXXX, XXX, XXX−XXX

The state-to-state rate coefficients are calculated by averaging the corresponding ICS, $\sigma_{vj\rightarrow v',j'}(E_c)$, over translational energy as

$$k_{vj\rightarrow v',j'}(T) = \left(\frac{8k_BT}{\pi\mu_R}\right)^{1/2}\left(\frac{1}{k_BT}\right)^2\int_0^\infty E_c\sigma_{vj\rightarrow v',j'}(E_c)e^{-E_c/k_BT}\,dE_c \quad (5)$$

where k_B is the Boltzmann constant and $\mu_R = m_O m_{H_2}/(m_{H_2} + m_O)$.

The thermal rate coefficients are then calculated by summing over all final (v', j') states and averaging over the initial states:

$$k(T) = \sum_p \frac{w_p}{Q_{v,j_p}(T)}\sum_{v,j_p}\sum_{v',j'} k_{vj_p\rightarrow v',j'}(T)g_{v,j_p}\exp\left(-\frac{E_{v,j_p}}{k_BT}\right) \quad (6)$$

where p is the diatomic parity (*ortho* and *para*), $j_p = j_{odd}$ or j_{even}, w_p is the nuclear spin weight of each species, Q_{v,j_p} is the rovibrational partition function including the nuclear spin weight,[28] E_{v,j_p} i sthe rovibrational energy of the (v, j_p) level, and g_{v,j_p} is its degeneration.

To check the convergence of the TDWP calculations of the reaction probability as a function of collision energy, additional calculations have been carried out using the TIQM methodology as implemented in the ABC code[29] for a series of total angular momentum values, J = 0, 10, 20, 30, 40, 50, and 60. The convergence parameters used in the TIQM calculations for the title reaction are given in Table 2.

Table 2. Parameters used in the TIQM Calculations

	$J = 0$	$J \geq 7$
hyperspherical maximal radius, ρ_{max}/a_0	25.0	25.0
no. of of sectors	400	400
no. of basis functions	364	2543
maximum projection quantum no., k_{max}	0	7
maximum rotational quantum no., j_{max}	30	30
maximum energy for basis set truncation, e_{max}/eV	3.0	3.0

QCT calculations have been carried out using the methodology described in previous works.[30,31] Specifically, to study the energy dependence of the reaction probability as a function of collision energy at fixed values of the total angular momentum, batches of 4 × 10^5 trajectories were run for the $O^+ + H_2(v$=0,1,j=0−2) reactions in the 4−830 meV collision energy range for J = 0, 40, and 60 following the procedure described in refs 31 and 32. Additional QCT calculations were carried out for impact parameter equal to 0 at the five collision energies of E_c = 22, 50, 137, 245, and 400 meV as described in refs 30 and 31. For the collision energy dependence of the integral cross section, 3 × 10^5 trajectories were run in the 0.05−0.3 eV collision energy range. The integration step size in the trajectories was chosen to be 0.03 fs, which guarantees a total energy conservation better than one part in 10^3. The trajectories were started and finished at an atom−diatom R distance of 10 Å. The rovibrational energies of the diatomic molecules were calculated by the semiclassical quantization of the action and their values were fitted to Dunham expansions in $v + 1/2$ and $j(j + 1)$.

3. RESULTS

Figure 1a shows the minimum energy path (MEP) calculated on the MMG PES[10] for a collinear configuration, $\widehat{OHH}$ α = 180°.

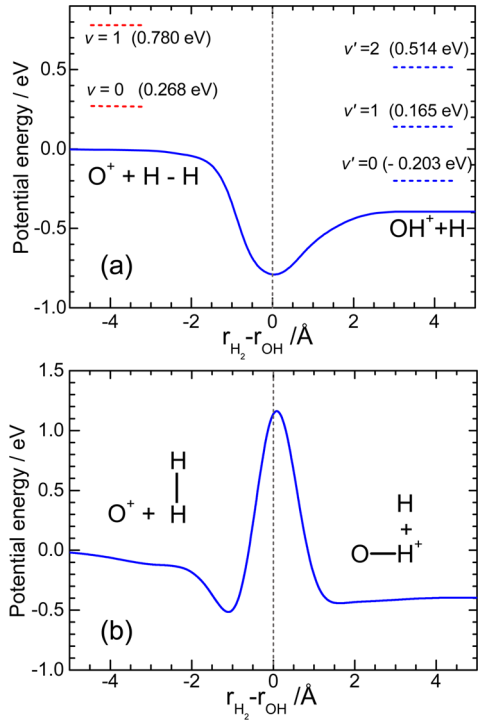

Figure 1. Minimum energy path for the $O^+ + H_2 \rightarrow OH^+ + H$ reaction calculated on the MMG PES[10] as a function of $r_{H_2} - r_{OH}$. (a) Collinear configuration, $\widehat{OHH}$ angle α = 180°. The dashed horizontal lines indicate the energy of the initial H_2 v = 0 and v = 1, and final OH^+ v' = 0, v' = 1, and v' = 2 vibrational states. (b) Perpendicular configuration $\widehat{OHH}$ angle α = 90°.

This MEP represents the potential energy of the OH_2^+ system as a function of a suitable reaction coordinate defined as $r_{H_2} - r_{OH}$, where r_{H_2} and r_{OH} are the H−H and O−H internuclear distances, respectively. In the potential energy minimization, the $\widehat{OHH}$ angle is maintained fixed. At large negative values of the reaction coordinate, r_{H_2} approaches the H_2 equilibrium distance for this reactant, whereas large positive values of the reaction coordinate correspond to r_{OH} values approaching the OH^+ equilibrium distance for this product. As expected, there is no barrier along the collinear reaction path and a deep well of about −0.8 eV from the reagent's minimum is found at r_{OH} = 1.141 Å and r_{H_2} = 1.182 Å. The reaction is exoergic by 0.4 eV (without taking into account the respective zero point energies). The energy levels of the vibrational states of reagents and products are indicated in the figure and show that the adiabatic reactions from $H_2(v$=0), yielding OH^+ in v' = 0 and v' = 1, are exoergic by 0.47 and 0.10 eV, respectively, whereas from $H_2(v$=1) yielding OH^+ in v' = 0, v' = 1, and v' = 2 are exoergic by 0.98 eV, 0.61, and 0.27 eV, respectively.

The corresponding MEP calculated for a perpendicular approach, $\widehat{OHH}$ α = 90°, is depicted in Figure 1b. As can be seen, a large barrier of about 1.2 eV, located at r_{OH} = 1.374 Å, r_{H_2} = 1.452 Å, appears in addition to shallow wells before and after the barrier. The depth of the entrance channel well (r_{H_2} = 0.794 Å and r_{OH} = 1.915 Å) is about −0.5 eV. These topographic features of the PES will clearly influence the dynamics

DOI: 10.1021/acs.jpca.5b00815
J. Phys. Chem. A XXXX, XXX, XXX−XXX

of the reaction, strongly favoring reactivity for collinear configurations and, thus, the H abstraction by the O^+ cation.

Reaction Probabilities. Figure 2 depicts the total reaction probability as a function of collision energy, $P^{J=0}_{v,j}(E_c)$, for the

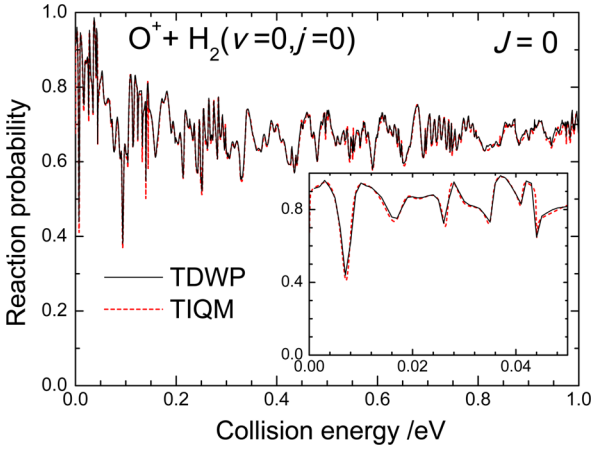

Figure 2. Total reaction probability as a function of collision energy calculated at $J = 0$ for the $O^+ + H_2(v=0,j=0)$ reaction. Black solid line: TDWP. Red dashed line: TIQM.

$O^+ + H_2(v=0,j=0)$ reaction calculated at total angular momentum $J = 0$ using the TDWP methodology. As expected, the $P^{J=0}_{0,0}(E_c)$ shows no threshold and several resonance peaks appear in the range of collision energies considered. The resonance structures may arise from the existence of the well in the MEP of the $O^+ + H_2$ reaction. As collision energy increases, the resonances become broader and less pronounced, reflecting the shortening of the lifetime of the collision complexes.

In the same figure, the TIQM results are also plotted. As can be seen, the agreement between both the TDWP and TIQM results is excellent even at very low collision energies. This is reassuring and indicates that the parameters used for the absorbing potential employed in the TDWP calculations have been finely tuned to avoid reflections at the edges of the grid, and that the number of Chebyshev iterations is large enough to get converged results. The present TDWP and TIQM results are in good agreement with all previous quantum mechanical calculations.[12,13,15]

The excellent agreement found in Figure 2 between TDWP and TIQM $J = 0$ reaction probabilities for the reaction $O^+ + H_2(v=0,j=0)$ extends to higher values of the total angular momentum J, as can be appreciated in Figure 3. The appearance of thresholds at increasing values of the collision energy due to the centrifugal barrier, which grows as $J(J + 1)$, is also evident in the figure. In addition, the number of oscillations in the $P^J_{0,0}(E_c)$ reduces and the resonances become broader. The calculations indicate that to obtained converged integral cross sections for high collision energies, a large number of partial waves are needed. In particular, to reach convergence at a collision energy of 1 eV, J must be at least 80.

In ref 12, Martínez et al. found a surprising and unexpected behavior in the collision energy dependence of the $J = 0$ reaction probability for $O^+ + H_2(v=0,j=0)$ reaction calculated by the QCT method when compared to TIQM calculations on the same PES (Figure 11 of ref 12). Two pronounced minima at 0.038 and 0.238 eV collision energies and a broad maximum between the two minima were found in the QCT $P^{J=0}_{0,0}(E_c)$ that were absent in the TIQM calculations. Only at the highest

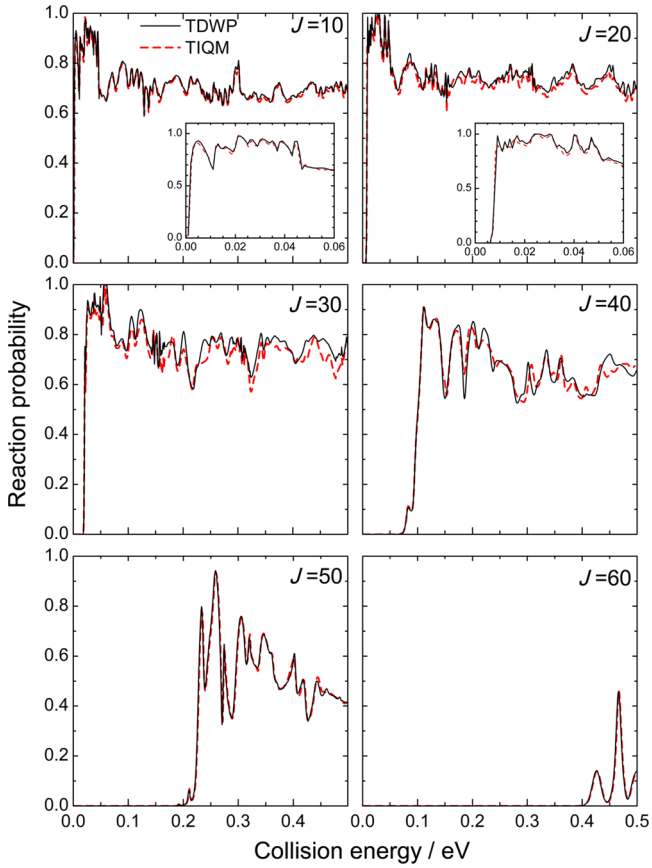

Figure 3. Total reaction probability as a function of collision energy calculated at $J = 10$, 20, 30, 40, 50, and 60 for the $O^+ + H_2(v=0,j = 0)$ reaction. Black solid line: TDWP. Red dashed line: TIQM.

collision energies do the QCT reaction probabilities seem to converge to the TIQM ones. As expected, the highly oscillatory behavior observed in the TIQM $P^{J=0}_{0,0}(E_c)$ due to quantum resonances (see above) could not be reproduced by the QCT calculations, but in addition, the coarse-grained shapes of the QCT and TIQM $P^{J=0}_{0,0}(E_c)$ were very different. The same kind of disagreement was found in calculations at other total angular momenta J between 10 and 40 for the $O^+ + H_2(v=0,j=0)$ reaction (Figure 12 in ref 12). The authors of ref 12 did not find a clear explanation for the different and peculiar behavior of the QCT $P^{J=0}_{0,0}(E_c)$.

The results of the present QCT calculations for the reactions $O^+ + H_2(v=0,j=0,1,2)$ are compared with the TDWP calculations in Figure 4. As can be seen, the present QCT calculations reproduce the shape of the reaction probability found previously by Martínez et al.[12] quite precisely for the $O^+ + H_2(v=0,j=0)$ reaction, and the two pronounced minima in the QCT $P^{J=0}_{0,0}(E_c)$ appear at about the same collision energies, 0.046 and 0.24 eV. As in ref 12, these two minima are not found in the TDWP results. However, the corresponding QCT calculations for initial $j = 1$ and $j = 2$ give rise to reaction probabilities without any pronounced minima, and with a smooth shape similar to that found in the TDWP calculations, apart from the quantum mechanical oscillations and somewhat larger values than those obtained in the TDWP calculations. As an additional observation, it is apparent from the figure that the rotational excitation in $H_2(v=0)$, at least for $J = 0$, has an overall negative effect on reactivity, and this behavior is also reproduced by the QCT calculations. This result is not surprising

DOI: 10.1021/acs.jpca.5b00815
J. Phys. Chem. A XXXX, XXX, XXX−XXX

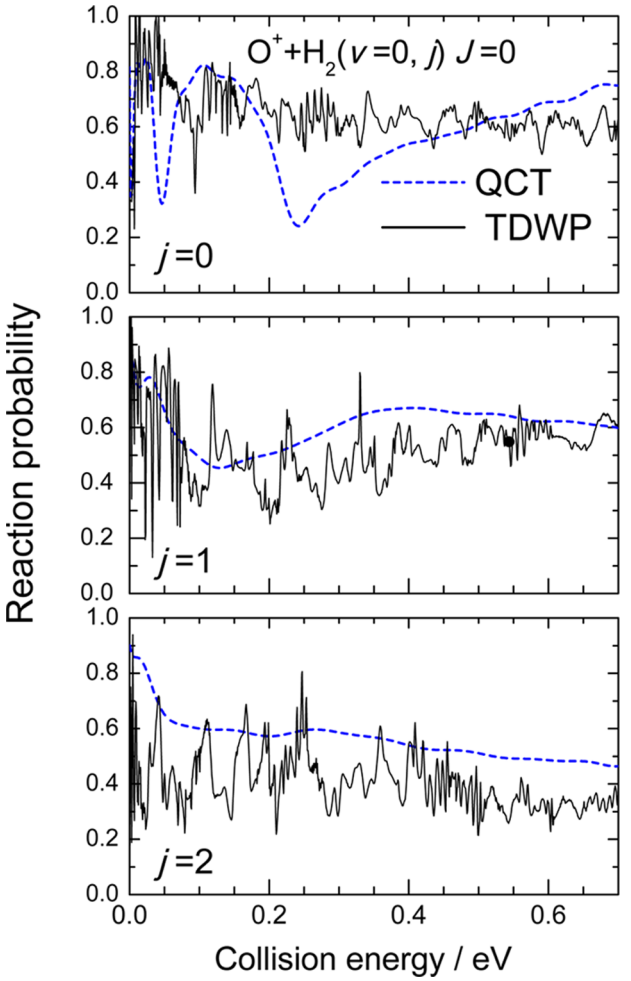

Figure 4. Total reaction probability as a function of collision energy calculated at $J = 0$ for the $O^+ + H_2(v=0, j)$ reactions. Top: $j = 0$. Middle: $j = 1$. Bottom: $j = 2$. Black solid line: TDWP. Blue dashed line: QCT.

because, as can be inferred from Figure 1, the reaction is strongly collinearly constrained and the barrier rises rapidly with bent geometries.

The investigation of the effect of vibrational excitation on the reaction probability deserves some attention. It is also worthwhile to examine if the peculiar shape of the QCT $P^{J=0}_{0,0}(E_c)$, in clear disagreement with the QM results, remains when H_2 is excited into $v = 1$. The comparison between TDWP and QCT, depicted in Figure 5, reveals the same type of discrepancy upon vibrational excitation: at similar collision energies, 0.056 and 0.28 eV, there are marked minima in strong resemblance with those found for the reaction in $v = 0$. Therefore, the presence of a coarse-grained structure in the QCT $P^{J=0}_{v,0}(E_c)$, at variance with the QM results, occurs whenever $j = 0$, for both $v = 0-1$ the H_2 vibrational states. Similar QCT calculations for $v = 1$ and $j = 1, 2$ (not shown) reveal that the peculiarities in the QCT $P^{J=0}_{v,j}(E_c)$ disappear.

The comparison of the results shown in the top panel of Figure 4 with those in Figure 5 for $J = 0$ indicate that reagent vibrational excitation has a mild positive net effect on reactivity, especially as the collision energy increases. A similar comment holds for values of J up to $J = 40$, as shown in Figure 6, where the $P^{J}_{v,0}(E_c)$ are compared for the reactions with H_2 in $v = 0$ and $v = 1$. For low values of the total angular momentum J and at

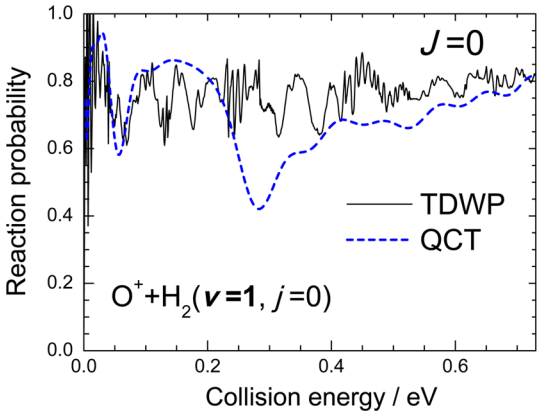

Figure 5. Total reaction probability as a function of collision energy calculated at $J = 0$ for the $O^+ + H_2(v=1,j=0)$ reaction. Black solid line: TDWP. Blue dashed line: QCT.

low collision energies ($\leq$0.4 eV), reaction probabilities and reaction thresholds are very similar, irrespective of the vibrational state of the H_2 molecules. At higher collision energies there is some propensity for larger reaction probabilities for reaction with $v = 1$. However, the situation changes drastically for large J values. For $J = 50$, the threshold for the reaction with $H_2(v=1)$ is somewhat smaller than that for $v = 0$ and the reaction probability is considerably reduced. When $J = 60$, the differences are indeed remarkable; the thresholds for $v = 0$ and $v = 1$ differ in >0.05 eV, and moreover, the magnitude of the $P^{J}_{v,0}(E_c)$ for $v = 0$ has greatly diminished and has become much smaller than that for $v = 1$ reaction. It can be expected that this behavior will manifest in the reaction cross section.

Integral Cross Sections. Summation of all partial wave contributions from $J = 0$ up to $J_{max} = 80$ yields state-to-state integral cross sections according to eq 3. Figure 7 depicts the integral cross sections summed over all final states as a function of collision energy, $\sigma_r(E_c)$, for the $O^+ + H_2(v=0,j=0,1,2)$ and $O^+ + H_2(v=1,j=0)$ reactions in the 10^{-3} to 1.0 eV collision energy range.

As expected for a barrierless exothermic reaction, the excitation functions decrease with increasing collision energy. It is interesting to note that the effect of the initial rovibrational state of the H_2 reactant on reactivity is found to be dependent on the collision energy. Thus, for collision energies above $\approx$0.3 eV, reactivity increases with the reagent vibrational and to a lesser extent with rotational excitation, whereas for collision energies below 0.3 eV, the cross sections decrease as j rises. The reason can be found in connection with the behavior discussed for the reaction probabilities. At low collision energies, rotational excitation of the H_2 molecule hinders the orientation of the reactant along the minimum energy path whose energy grows quickly with the disruption of the collinear arrangement. However, as collision energy increases, the cone of acceptance broadens and rotation does not hamper the access to the well and hence to product formation.

The effect of vibrational excitation cannot be explained on the same basis. The comparison of the excitation for $O^+ + H_2(v=0,j=0)$ and $O^+ + H_2(v=1,j=0)$ reaction, portrayed in the upper panel of Figure 7, reveals that while at low energies the differences are relatively small, above 0.3 eV both curves diverge and the reactivity for reaction in $v = 1$ is clearly larger. This result could be anticipated by inspection of Figure 6. As can be seen, by $E_c \approx 0.3$ eV, partial waves in the 50–60 J range

DOI: 10.1021/acs.jpca.5b00815
J. Phys. Chem. A XXXX, XXX, XXX−XXX

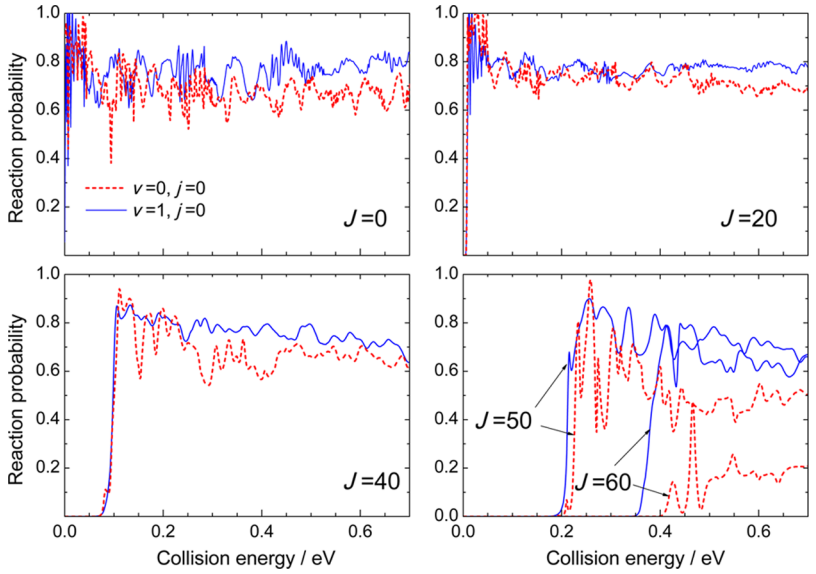

Figure 6. Comparison of TDWP total reaction probabilities as a function of collision energy for the $O^+ + H_2(v=0,j=0)$ (dashed red lines) and $O^+ + H_2(v=1,j=0)$ (solid blue lines) reactions at the indicated J values.

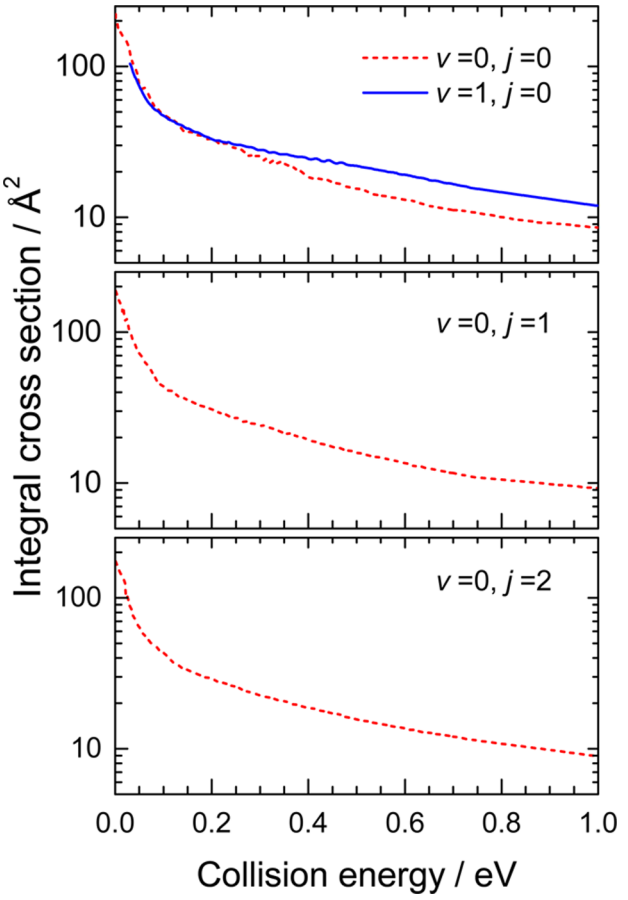

Figure 7. Total reaction cross-section as a function of collision energy for the $O^+ + H_2$ reaction with the H_2 at the specified v, j initial rovibrational states.

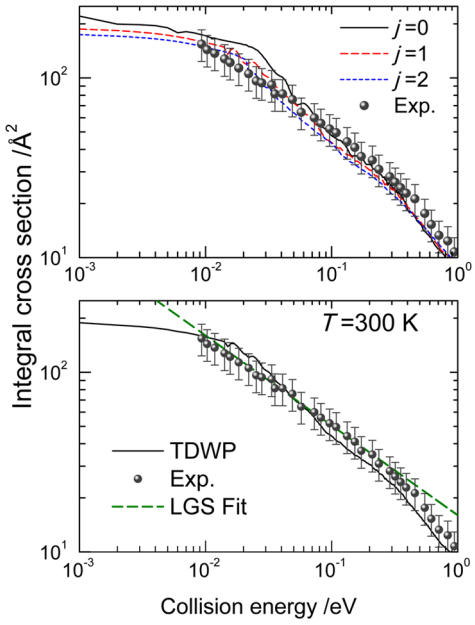

Figure 8. Top: total reaction cross section as a function of collision energy for the $O^+ + H_2(v=0,j)$ reactions. Solid black line: j = 0. Red dashed line: j = 1. Blue short-dashed line: j = 2. Solid circles: experimental results from ref 7. Bottom: Total reaction cross section as a function of collision energy for the $O^+ + H_2(v=0,\langle j\rangle)$ reaction averaged over the thermal rotational population at 300 K. Black solid line: TDWP. Solid circles: experimental results from ref 7. Green dashed line: Langevin model, $\sigma_r(E_c) = AE_c^{-1/2}$; A = 16 Å^2 eV$^{1/2}$.

start to contribute, and for these J values and above the reactivity is considerably enhanced upon excitation into v = 1. We will see below an explanation of this behavior.

The top panel of Figure 8 depicts the comparison between the experimental results of Burley et al.,[7] corresponding to the reaction of O^+ with thermal H_2 at T = 300 K, and the TDWP excitation functions for j = 0, 1, 2. By and large, the agreement between the theoretical curves and the experimental thermal cross section is fairly good. As commented on above, there is a mild effect associated with reagent rotational excitation on the shape of the cross section as a function of E_c, with a propensity for smaller cross sections as initial j increases, especially at collision energies below 0.1 eV. The larger divergence between experiment and the various j excitation functions is found for

DOI: 10.1021/acs.jpca.5b00815
J. Phys. Chem. A XXXX, XXX, XXX−XXX

the reaction with initial $j = 0$ in the collision energy region between 10^{-2} and 6×10^{-2} eV, where the TDWP results clearly overestimate the experimental values.

By averaging the $O^+ + H_2(v{=}0,j{=}0,1,2)$ excitation functions with the corresponding Boltzmann weights (including the nuclear spin weights) at $T = 300$ K for n-H_2 ($j = 0$, 14.22%; $j = 1$, 72.78%; $j = 2$, 13.00%), we can directly compare the resulting excitation function with the experimental measurements by Burley et al.[7] This comparison is shown in the bottom panel of Figure 8. A good agreement is found between the present TDWP calculations and the experimental values for collision energies between 0.01 eV and ≈0.1 eV, but at higher collision energies (>0.1 eV), the TDWP excitation function falls somewhat below the experimental points although within the experimental error bars.

The TDWP excitation function departs noticeably from the behavior predicted by the Langevin model at the lowest collision energies (<0.01 eV), for which there are no experimental data. As discussed by Burley et al.,[7] the formula $\sigma_r = CE_c^{-1/2}$, where C is proportional to the square root of the polarizability, accounts very well for the measured data below 0.3 eV. Above that energy, the Langevin model clearly overestimates the experimental cross sections. The most remarkable fact, already pointed out in ref 16, is the leveling off of the TDWP $\sigma_r(E_c)$ at energies below 0.01 eV, in clear contrast with the monotonic behavior predicted by the Langevin model. Unfortunately, there are no measurements in that low energy region, and it cannot be concluded whether the deviation from the simple albeit venerable Langevin model is due to the inherent limitations of this model or to the present theoretical treatment. As commented on already, the TDWP results have been carefully checked with TIQM calculations, in principle less prone to propagation errors than the TD method at low energies, and the agreement between the results from the two methodologies was found to be excellent down to 10^{-3} eV collision energy. However, the PES and, in particular its long-range, may not be sufficiently accurate to account for the cross sections or rate coefficients at those small energies/temperatures.

It must be added that the present TDWP results are in very good agreement with the previous TIQM results by Martínez et al.[12] for collision energies in the range 0.038−0.7 eV and with the TDWP-CC results by Xu et al.[15] for collision energies in the range 0.05−0.7 eV. This fact, although not surprising because all the calculations have been conducted on the same PES, is reassuring with regard to the quality of past and present calculations.

Thermal Rate Coefficients. With the TDWP excitation function averaged over $v = 0$, $j = 0$, 1, 2 H_2 rovibrational states, thermal rate coefficients have been calculated according to eq 6 for temperatures ranging from 200 K up to 1000 K and are shown in Figure 9 as an Arrhenius plot. As expected, the rate coefficients are fairly constant in the 200−500 K. For higher temperatures, the TDWP $k(T)$ decrease slightly, similarly to the previous QCT rate coefficients calculated by Martínez and coworkers.[10] At $T = 300$ K, the TDWP rate coefficient is 1.65×10^{-9} cm^3 s^{-1}, which coincides with the experimental value of $1.67 \pm 0.3\times 10^{-9}$ cm^3 s^{-1} [7] and somewhat smaller than that found in the QCT calculations (1.71×10^{-9} cm^3 s^{-1}) by Martínez et al.[10] In spite of the small discrepancies between the experimental and TDWP excitation functions, once the average over the collision energy is carried out, the agreement between the experimental and calculated $k(T = 300\ \text{K})$ is very good.

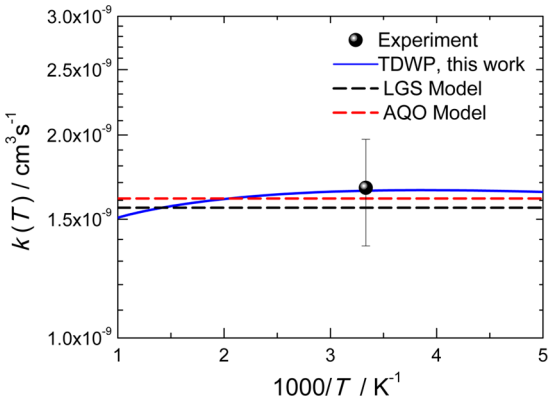

Figure 9. Thermal rate constants for the $O^+ + H_2$ reaction. Blue solid line: TDWP. Solid circle: experimental result from ref 7. Black dashed line: Langevin model. Red dashed line: AQO model.

Figure 9 also displays the rate coefficients given by the simple Langevin model[19,20] and that calculated by Burley et al.[7] including the average charge−quadrupole anisotropic interaction (the so-called anisotropic quadrupole orientation, AQO model),[33] which is relevant for $j \neq 0$. Both, the Langevin and AQO model, predict a strictly constant $k(T)$ and they are within the error bar of the experimental datum at 300 K and not far from the TDWP prediction on the MMG PES. At temperatures above 500 K, the quantum scattering prediction starts to decrease very slowly and at $T = 1000$ K, $k(T) = 1.5 \times 10^{-9}$ cm^3 s^{-1}.

4. DISCUSSION

Classical versus Quantum Reaction Probabilities. The peculiar behavior of the QCT $P^{J=0}_{v,0}(E_c)$ for the reaction with $H_2(v{=}0,1,j{=}0)$ depicted in Figures 4 and 5 deserves some attention. The fact that identical results were also obtained by Martínez et al.,[12] using a completely different QCT code, rules out the possibility of a systematic error in the calculations. Because trajectories are more sensitive to the details of the PES, especially at low collision energies, than QM calculations, it is pertinent to examine the origin of those broad undulations and trace them back to the topography of the PES, and to explain why the agreement between QCT and TDWP reaction probabilities improves substantially for the reactions with initial $j = 1$ and $j = 2$. For this purpose, we have carried out detailed analysis of individual trajectories calculated for collision energies at the several minima and maxima found in the QCT $P^{J=0}_{0,0}(E_c)$ for the $O^+ + H_2(v{=}0,j{=}0)$ reaction. Specifically, there are minima in the reaction probability for initial $v = 0$ at collision energies 50 and 245 meV and maxima at 22 and 137 meV. For $E_c > 250$ meV, the reaction probability grows monotonically with values comparable to those obtained in the QM calculations (top panel of Figure 4). Very similar behavior of alternating maxima and minima at almost the same collision energy, barely shifted toward higher collision energies, is found for the $P^{J=0}_{1,0}(E_c)$, as shown in Figure 5. It must be concluded that, whatever causes this effect, it has to be related to the coupling of the translational energy (or the relative velocity of approach) and some orientational effect of the PES. It must be recalled that the side-on attack of O^+ to H_2 faces a very high barrier, whereas a head-on, collinear attack has no barrier, as shown in Figure 1.

In the absence of rotation the orientational effect of the PES on the $H_2(j{=}0)$ molecule approaching the O^+ atom must

DOI: 10.1021/acs.jpca.5b00815
J. Phys. Chem. A XXXX, XXX, XXX−XXX

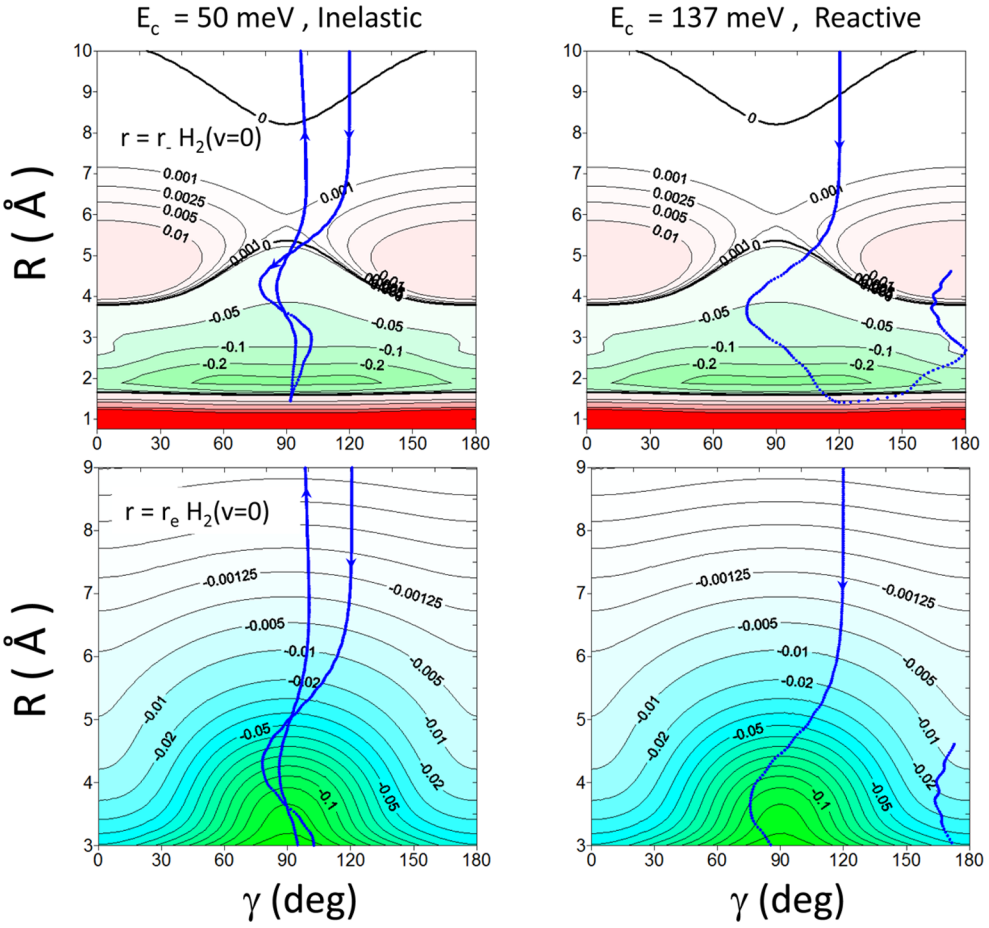

Figure 10. Contour plots of the potential in the entrance channel as a function of the reactant's Jacobi coordinates, R and γ at a fixed internuclear distance, r, corresponding to the inner $H_2(v=0,j=0)$ turning point, r_- (top panel) and to the equilibrium distance, r_e (bottom panel). The zero energy of each plot corresponds to the asymptotic value at the indicated internuclear distances. On top of these plots, two trajectories: one inelastic, at E_c = 50 meV (left panel) and one reactive, at E_c = 137 meV (right panel) are represented. Notice that the trajectories shown in the upper and lower panel are the same. See text for more details.

determine the relative orientation (the value of the Jacobi γ angle) when the strong interaction takes place, immediately before the H abstraction by O^+ (hereinafter interaction region). If that orientation is favorable, that is, close to collinearity (low barrier), reaction will take place; if, instead, the orientation is side-on, the barrier will prevent the reaction from occurring. One can expect that collisions starting at attacking angles near 0° or 180° will give rise to reaction, whereas those starting near 90° will be inelastic. However, trajectories whose initial attacking angle, γ_0, is in the range 60°−80° (and 100°−120°) are susceptible to experience torques that may cause favorable or unfavorable orientations en route to the transition state. The interesting point is that for trajectories with attacking angles in the 60°−80° range, the orientation of the $H_2(j=0)$ internuclear axis that the molecules exhibit when they reach the interaction region depends on the velocity of approach (and hence on the collision energy), causing the presence of marked minima in the QCT $P_{v,0}^{J=0}(E_c)$ for the $O^+ + H_2(v,j=0)$ reactions.

Figure 10 shows contour plots of the PES in the $R-\gamma$ Jacobi coordinates for r values corresponding to the inner turning point of H_2 in v = 0, r_- = 0.633 Å (top panels) and to the H_2 equilibrium distance, r_e = 0.741 Å (bottom panels). On top of each contour plot, a trajectory started at an initial angle γ_0 = 120°, and $H_2(v=0,j=0)$ has been plotted. We have chosen two collision energies, which correspond to the first minimum in the $P_{0,0}^{J=0}(E_c)$ depicted in the top panel of Figure 4, at E_c = 50 meV (showing an inelastic trajectory), and the following maximum at $E_c \approx$ 137 meV (showing a reactive trajectory). In the Supporting Information, PES contour plots and trajectories are depicted for five different collision energies corresponding to each of the maxima and minima of the $P_{0,0}^{J=0}(E_c)$ along with the corresponding movies of the trajectories.

The contour plots show that the shallow C_{2v} van der Waals well in the entry channel causes the asymmetry of the potential even at R > 6 Å. This effect is particularly noticeable at the inner turning point of the $H_2(v=0,j=0)$ (upper panels) where two shallow and small maxima centered at γ = 0° and 180° are found. The van der Waals well is not deep enough to trap the trajectory, but it changes the γ contribution of the relative velocity and orients the trajectory toward side-on configurations. As can be seen in the animations included in the Supporting Information, the induced rotation is rather subtle, and the number of successive changes of directions is a function of the relative velocity. The minima pattern in the $P_{0,0}^{J=0}(E_c)$ is caused by trajectories with attacking angles in the range 60°−80° that experience one (E_c = 245 meV) and three (E_c = 50 meV) changes of direction and reaches the interaction region at perpendicular (and thus repulsive) geometries.

The effect just described is purely classical and implies collisions with strictly rotationless H_2 molecules. Once rotation

DOI: 10.1021/acs.jpca.5b00815
J. Phys. Chem. A XXXX, XXX, XXX−XXX

is included in the H_2 molecule, these orientational effects induced by the PES topography vanish and the QCT $P^{J=0}(E_c)$ becomes smooth, in agreement with the TDWP $P^{J=0}(E_c)$ (apart from the ubiquitous high frequency oscillations due to resonances). In the QM case for the reaction with $j = 0$, the effective potential is not a local magnitude and can only be conceived as averaged over all possible orientations that are equiprobable for $j = 0$. Once the potential is averaged, the PES and gradient local features lose their classical dynamical meaning. The effect is, in a way, similar to the classical case when rotation is included.

Effect of Reagent Vibrational Excitation on Reactivity. For a barrierless, exothermic reaction, the effect of vibrational excitation is expected to play a small role—sometimes negative—on the reactivity. The reaction probabilities and integral cross sections, respectively, shown in Figures 6 and 7, confirm that this is the case for the title reaction. The reagent's vibrational excitation into $v = 1$ has a mild effect on reaction probabilities or cross sections below 0.2 eV, in spite of the fact that the exothermicity of the reaction increases substantially upon vibrational excitation (Figure 1). More surprising, however, is the finding that at collision energies above ≈0.2−0.3 eV the excitation function for the reaction with $v = 1$ clearly lies above that with $v = 0$, as shown in Figure 7. One would expect that at sufficiently high collision energies the effect on the overall reactivity would be even less than that at lower E_c. The explanation of this deviation can be found in the striking differences between the reaction probabilities for total angular momenta $J \geq 50$. The distinct results for $J = 60$, shown in Figure 6, illustrate very well this finding. Not only the threshold but also the magnitude of the reaction probability is hugely enhanced in the reaction with $v = 1$. One may wonder if such an effect also occurs in the classical calculations: the corresponding QCT comparison of the $v = 0$ and $v = 1$ reaction probabilities for $J = 40$ and 60 is shown in Figure 11. As can be

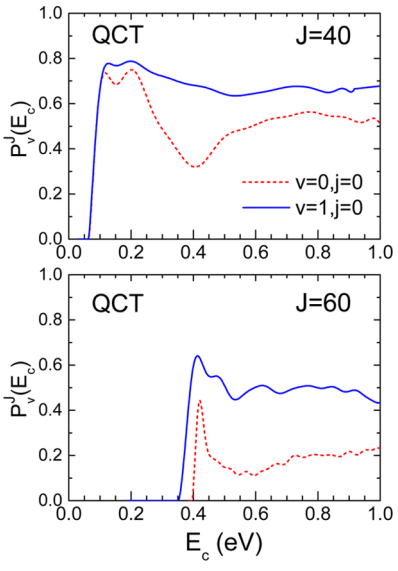

Figure 11. QCT total reaction probability as a function of collision energy for $J = 40$ (upper panel) and $J = 60$ (bottom panel). Dashed lines: $O^+ + H_2(v=0,j=0)$ reaction. Solid lines: $O^+ + H_2(v=1,j=0)$ reaction.

seen, the effect is almost quantitatively reproduced by the QCT calculations. Therefore, it should be a common reason for the differences between the $v = 0$ and $v = 1$ reaction probabilities for $J > 50$.

Because the differences in the reactivity occur at relatively high values of J (or l, the orbital angular momentum), it can be expected that the ultimate reason for this behavior would lie in the effective potential in the entrance channel, which includes the J (or l)-dependent centrifugal barrier. Therefore, for the reactions of O^+ atoms with $H_2(v=0)$ and $H_2(v=1)$ the shapes of the J-dependent effective potentials and, in particular, its height must be different.

We can define an effective (long-range) potential as a function of the atom−diatom distance, R, for a given J as the diagonal matrix element of the full potential energy between the initial H_2 rovibrational functions,

$$V_{vj}^{\text{eff}}(R) = \langle \chi_{vj}(r) Y_{j\Omega} | V(r,R,\gamma) | \chi_{vj}(r) Y_{j\Omega} \rangle + \frac{J(J+1)\hbar^2}{2\mu R^2} - \langle V(r,R\rightarrow\infty) \rangle_{v,j} \quad (7)$$

where the brackets indicate the integration over r and γ at a fixed value of R (R, r, and γ are Jacobi coordinates), and the last term ensures that the average potential is zero asymptotically. Figure 12 portrays the effective potentials for the O^+ +

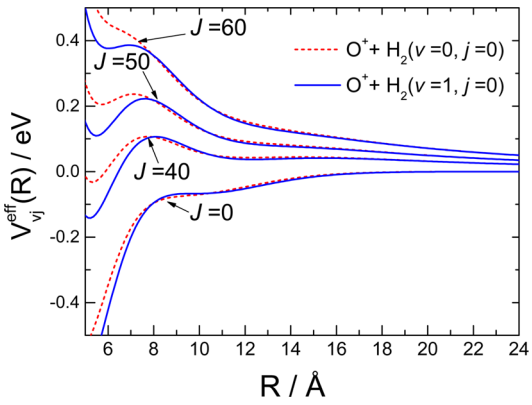

Figure 12. Effective potentials $V_{vj}^{\text{eff}}(R)$ as defined in the text (eq 7). Blue solid lines: $O^+ + H_2(v=1,j=0)$. Red dashed lines: $O^+ + H_2(v=0,j=0)$.

$H_2(v=0,j=0)$ and $O^+ + H_2(v=1,j=0)$ reactions calculated at $J = 0$, 40, 50, and 60 as a function of R. As can be appreciated, the $v = 0$ and $v = 1$ effective potentials are very similar up to $J \approx 40$. However, for $J \geq 50$ and $R < 8$ Å, the effective potentials for $O^+ + H_2(v=0,j=0)$ grows faster than those for $O^+ + H_2(v=1,j=0)$ and gives rise to a higher barrier and, consequently, to a much lower reactivity. Notice, however, that this potential is only meaningful at sufficiently high R distances.

5. CONCLUSIONS

We have carried out comprehensive calculations to study the dynamics of the $O^+ + H_2$ reaction employing an accurate coupled channel time-dependent wave packet (TDWP) methodology. All the calculations have been performed on the *ab initio* PES developed by Martínez et al.[10] Time-independent quantum mechanical (TIQM) calculations have also been carried out to compare with the TDWP calculations, especially at the lowest collision energies to assess the accuracy of the latter. Reaction probabilities, integral cross sections, and rate coefficients have been determined for $O^+ + H_2(v=0,j=0, 1, 2)$ and $O^+ + H_2(v=1,j=0)$

DOI: 10.1021/acs.jpca.5b00815
J. Phys. Chem. A XXXX, XXX, XXX−XXX

reactions. The present results, when coincident, are found in good agreement with those from previous calculations.

The main goal of the present study is to elucidate the role of reagent rotational and vibrational excitation on reactivity. It has been found that H_2 rotation (j = 1, 2) has a very small effect on the overall reactivity that is only noticeable at collision energies below 10^{-2} eV, where it causes a decrease of the integral cross section. In turn, vibrational excitation has an interesting effect: at collision energies below 0.3 eV the total reaction cross section is almost unaltered when H_2 is promoted to v = 1. However, at higher collision energies, the cross section increases with vibrational excitation. This effect has been traced back to the shapes and magnitudes of the reaction probability. Whereas the collision energy dependence of the v = 0 and v = 1 reaction probabilities for J < 50 are very similar and have the same threshold, for J values above ≈50 the energy threshold becomes considerably smaller and moreover the probabilities are much larger in the case of the reaction with v = 1 molecules. This effect has also been found in the QCT calculations. The reason for this behavior can be found in the effective potential in the entrance channel arising from the composition of the centrifugal and electronic potentials. The resulting barrier for the reaction with H_2 in v = 1 is smaller that that found for v = 0 as long as J > 50.

In addition, QCT calculations have been carried out to gain a more intuitive understanding of the nuclear dynamics of the title reaction. In particular, the peculiar shape found for the QCT reaction probabilities as a function of collision energy for the reaction with $H_2(v{=}0,j{=}0)$, featuring the presence of several pronounced minima which are absent in the QM calculations, has been explained in terms of the coupling between collision energy (or the velocity of mutual approach) and the topography of the PES. The analysis of individual trajectories indicates that the potential induces a torque in the H_2 molecule, such that if the resulting orientation is favorable when the strong interaction takes place, reaction occurs and otherwise just causes an inelastic collision. The succession of maxima and minima in the J = 0 reaction probability is also found for the reaction with H_2 in v = 1 but disappears when some rotation is included in the reagents. This behavior, which is in contrast with that found in QM calculations, is due to the local character of the potential in the classical calculations.

Calculated excitation functions and thermal rate coefficients have been compared with the existing experimental results with a general good agreement found, indicating the accuracy of the PES and of the dynamical calculations.

■ ASSOCIATED CONTENT

Supporting Information

(a) TDWP cross sections and thermal rate coefficients, (b) contour plots of the potential in R, γ Jacobi coordinates. On top of each plot, a typical trajectory has been represented at various collision energies. For each of them, a movie is included. This material is available free of charge via the Internet at http://pubs.acs.org.

■ AUTHOR INFORMATION

Corresponding Author

*E-mail: lbanares@ucm.es.

Notes

The authors declare no competing financial interest.

■ ACKNOWLEDGMENTS

N.B. acknowledges a grant by Universidad Complutense de Madrid under the program "Programa de doctores y tecnólogos en la UCM-Grupo Santander". Financial support from the Scientific and Technological Research Council of TURKEY (TUBITAK) (Project No. TBAG-112T827) and FIRAT University Scientific Research Projects Unit (Project No. FF.14.20) is gratefully acknowledged. TDWP computations have been performed on the High Performance and Grid Computing Center (TR-Grid) at ULAKBIM/TURKEY and in the parallel facilities at CESGA computing center, through ICTS grants, which are acknowledged. The authors acknowledge funding by the Spanish Ministry of Economy and Competitiveness (grants CTQ2008-02578/BQU, FIS2011-29596-C02, CTQ2012-37404-C02 and Consolider Ingenio 2010 CSD2009-00038). O.R. and N.B. also acknowledge CSIC for a traveling grant I-LINK0775. J.K. expresses his gratitude to the US National Science Foundation (grants to Prof. Millard Alexander No. CHE-1213332).

■ REFERENCES

(1) Duley, W. W.; Williams, D. A. *Interstellar Chemistry*; Academic: New York, 1984.

(2) Armentrout, P. Kinetic Energy Dependence of Ion−Molecule Reactions: Guided Ion Beams and Threshold Measurements. *Int. J. Mass Spectrom.* **2000**, *200*, 219.

(3) Fehsenfeld, F. C.; Schmeltekopf, A. L.; Ferguson, E. E. Thermal-Energy Ion-Neutral Reaction Rates. VII. Some Hydrogen-Atom Abstraction Reactions. *J. Chem. Phys.* **1967**, *46*, 2802−2808.

(4) Kim, J. K.; Theard, L. P.; Huntress, W. T. ICR Studies of some Hydrogen Atom Abstraction Reactions: $X^+ + H_2 \rightarrow XH^+ + H$. *J. Chem. Phys.* **1975**, *62*, 45.

(5) Smith, D.; Adams, N. G.; Miller, T. M. A Laboratory Study of the Reactions of N^+, N_2^+, N_3^+, N_4^+, O^+, O_2^+, and NO^+ Ions with Several Molecules at 300 K. *J. Chem. Phys.* **1978**, *69*, 308.

(6) Federer, W.; Villinger, H.; Howorka, F.; Lindinger, W.; Tosi, P.; Bassi, D.; Ferguson, E. Reaction of O^+, CO^+, and CH^+ Ions with Atomic Hydrogen. *Phys. Rev. Lett.* **1984**, *52*, 2084.

(7) Burley, J.; Ervin, K. M.; Armentrout, P. Translational Energy Dependence of $O^+(^4S) + H_2(D_2, HD)OH^+(OD^+) + H(D)$ from Thermal Energies to 30 eV c.m. *Int. J. Mass Spectrom. Ion Processes* **1987**, *80*, 153.

(8) Sunderlin, L.; Armentrout, P. Temperature Dependence of the Reaction of O^+ with HD. *Chem. Phys. Lett.* **1990**, *167*, 188.

(9) Flesch, G. D.; Ng, C. Y. Absolute Total Cross Sections for the Charge Transfer and Dissociative Charge Transfer Channels in the Collisions of $O^+(^4S)+H_2$. *J. Chem. Phys.* **1991**, *94*, 2372.

(10) Martínez, R.; Millán, J.; González, M. Ab initio Analytical Potential Energy Surface and Quasiclassical Trajectory Study of the $O^+(^4S)+H_2 \rightarrow OH^+(X^3\Pi)+H(^2S)$ Reaction and Isotopic Variants. *J. Chem. Phys.* **2004**, *120*, 4705.

(11) Martínez, R.; Sierra, J. D.; González, M. Cross Sections of the $O^+ + H_2 \rightarrow OH^+ + H$ Ion−Molecule Reaction and Isotopic Variants (D_2, HD): Quasiclassical Trajectory Study and Comparison with Experiments. *J. Chem. Phys.* **2005**, *123*, 174312.

(12) Martínez, R., Lucas, J. M., Giménez, X., Aguilar, A., González, M. Exact Quantum Dynamics Study of the $O^+ + H_2(v{=}0,j{=}0) \rightarrow OH^+ + H$ Ion−Molecule Reaction and Comparison with Quasiclassical Trajectory Calculations *J. Chem. Phys.* **2006**, *124*, 144301.

(13) Martínez, R.; Sierra, J. D.; Gray, S. K.; González, M. Time Dependent Quantum Dynamics Study of the $O^+ + H_2(v{=}0,j{=}0) \rightarrow OH^+ + H$ Ion−Molecule Reaction and isotopic variants (D_2,HD. *J. Chem. Phys.* **2006**, *125*, 164305.

(14) Kłos, J.; Bulut, N.; Akpinar, S. Nonreactive Scattering of the $O^+ + H_2$: A Time Dependent Wave Packet Approach. *Chem. Phys. Lett.* **2012**, *532*, 22.

DOI: 10.1021/acs.jpca.5b00815
J. Phys. Chem. A XXXX, XXX, XXX−XXX

(15) Xu, W.; Li, W.; Lv, S.; Zhai, H.; Duan, Z.; Zhang, P. Coriolis Coupling Effects in $O^+(^4S) + H_2(X) \rightarrow OH^+(X^3\Pi) + H(^2S)$ Reaction and Its Isotopic Variants: Exact Time-Dependent Quantum Scattering Study. *J. Phys. Chem. A* **2012**, *116*, 10882−10888.
(16) Gómez-Carrasco, S.; Godard, B.; Lique, F.; Bulut, N.; Kłos, J.; Roncero, O.; Aguado, A.; Aoiz, F. J.; Castillo, J. F.; Goicoechea, J. R.; et al. OH^+ in Astrophysical Media: State-to-State Formation Rates, Einstein Coefficients and Inelastic Collision Rates with He. *Astrophys. J.* **2014**, *794*, 33.
(17) Gillen, K. T.; Mahan, B. H.; Winn, J. S. Dynamics of the $O^+ + H_2$ Reaction. I. Reactive Scattering of $O^+(^4S_{3/2})$ at Relative Energies below 15 eV. *J. Chem. Phys.* **1973**, *58*, 5373.
(18) Gillen, K. T.; Mahan, B. H.; Winn, J. S. Dynamics of the $O^+ + H_2$ Reaction. II. Reactive and Nonreactive Scattering of $O^+(^4S_{3/2})$ at Relative Energies above 13 eV. *J. Chem. Phys.* **1973**, *59*, 6380.
(19) Langevin, P. A. Fundamental Formula of Kinetic Theory. *Ann. Chim. Phys.* **1905**, *5*, 245.
(20) Gioumousis, G.; Stevenson, D. P. Reactions of Gaseous Molecule Ions with Gaseous Molecules. V. Theory. *J. Chem. Phys.* **1958**, *29*, 294.
(21) Gómez-Carrasco, S.; Roncero, O. Coordinate Transformation Methods to Calculate State-to-State Reaction Probabilities with Wave Packet Treatments. *J. Chem. Phys.* **2006**, *125*, 054102.
(22) Zanchet, A.; Roncero, O.; González-Lezana, T.; Rodríguez-López, A.; Aguado, A.; Sanz-Sanz, C.; Gómez-Carrasco, S. Differential Cross Sections and Product Rotational Polarization in A + BC Reactions Using Wave Packet Methods: $H^+ + D_2$ and Li + HF Examples. *J. Phys. Chem. A* **2009**, *113*, 14488.
(23) Zanchet, A.; González-Lezana, T.; Aguado, A.; Gómez-Carrasco, S.; Roncero, O. Nonadiabatic State-to-State Reactive Collisions among Open Shell Reactants with Conical Intersections: The $OH(^2\Pi)$ + $F(^2P)$ Example. *J. Phys. Chem. A* **2010**, *114*, 9733.
(24) Gonzalez-Sanchez, L.; Vasyutinskii, O.; Zanchet, A.; Sanz-Sanz, C.; Roncero, O. Quantum Stereodynamics of Li + HF Reactive Collisions: The Role of Reactants Polarization on the Differential Cross Section. *Phys. Chem. Chem. Phys.* **2011**, *13*, 13656−13669.
(25) Aslan, E., Bulut, N., Castillo, J. F., Banares, L., Aoiz, F. J., Roncero, O. Accurate Time-Dependent Wave Packet Study of the H^+ + LiH Reaction at Early Universe Conditions *Astrophys. J.* **2012**, *759*, 31.
(26) Alagia, M.; Balucani, N.; Cartechini, L.; Casavecchia, P.; Volpi, G. G.; Aoiz, F. J.; Bañares, L.; Allison, T. C.; Mielke, S. L.; Truhlar, D. G. Dynamics of the $Cl+H_2/D_2$ Reaction: a Comparison of Crossed Molecular Beam Experiments with Quasiclassical Trajectory and Quantum Mechanical Calculations. *Phys. Chem. Chem. Phys.* **2000**, *2*, 599.
(27) Aoiz, F. J.; Sáez-Rábanos, V.; Martínez-Haya, B.; González-Lezana, T. Quasiclassical Determination of Reaction Probabilities as a Function of the Total Angular Momentum. *J. Chem. Phys.* **2005**, *123*, 094101.
(28) Jambrina, P. G., Lara, M., Menendez, M., Launay, J. M., Aoiz, F. J. Rate Coefficients from Quantum and Quasi-Classical Cumulative Reaction Probabilities for the $S(^1D) + H_2$ Reaction *J. Chem. Phys.* **2012**, *137*, 164314.
(29) Skouteris, D.; Castillo, J.; Manolopoulos, D. ABC: A Quantum Reactive Scattering Program. *Comput. Phys. Commun.* **2000**, *133*, 128.
(30) Aoiz, F.; Herrero, V.; Sáez Rábanos, V. Quasiclassical State to State Reaction Cross Sections for the $D+H_2$. Formation and Characterization of Short-Lived Collision Complexes. *J. Chem. Phys.* **1992**, *97*, 7423.
(31) Aoiz, F. J.; Bañares, L.; Herrero, V. J. Recent Results from Quasiclassical Trajectory Computations of Elementary Chemical Reactions. *J. Chem. Soc., Faraday Trans.* **1998**, *94*, 2483.
(32) Carmona-Novillo, E.; González-Lezana, T.; Roncero, O.; Honvault, P.; Launay, J.-M.; Bulut, N.; Aoiz, F. J.; Bañares, L.; Trottier, A.; Wrede, E. On the Dynamics of the $H^+ + D_2(v=0, j=0) \rightarrow$ HD+ D^+ Reaction: A Comparison between Theory and Experiment. *J. Chem. Phys.* **2008**, *128*, 014304.
(33) Su, T.; Bowers, M. T. Ion-Polar Molecular Collisions: The Average Quadrupole Orientation Theory. *Int. J. Mass Spectrom. Ion Processe.* **1975**, *17*, 309.

DOI: 10.1021/acs.jpca.5b00815
J. Phys. Chem. A XXXX, XXX, XXX−XXX